QUASI STEADY-STATE HURRICANES REVISITED

John Persing[a], Michael T. Montgomery[a*], Roger K. Smith[b], and James C. McWilliams[c]

[a]*Department of Meteorology, Naval Postgraduate School, Monterey, California, USA*
[b]*Meteorological Institute, Ludwig-Maximilians University of Munich, Munich, Germany*
[c]*Department of Atmospheric and Oceanic Sciences, University of California at Los Angeles, Los Angeles, California, USA*

ABSTRACT

We revisit the theoretical possibility of long-term, sustained tropical cyclone solutions using a state-of-the-art numerical model that incorporates the most recent observational guidance for subgrid scale parameters and air-sea exchange coefficients of heat and momentum. Emphasis is placed on the realism of such solutions and the sources of cyclonic relative angular momentum (RAM) that are necessary to replenish that lost by friction at the surface. For simplicity, we confine our attention to strictly axisymmetric numerical experiments.

We are able to replicate Hakim's long-term simulation of a quasi-steady state cyclone in a 1500 km radial domain. The structure of the wind field is found to be somewhat realistic compared to observations, but sustained by unrealistic processes. Artificial sources of cyclonic RAM are quantified and the lateral damping of the anticyclonic wind near the outer boundary is found to make the largest contribution to the source of cyclonic RAM. When the domain size is extended to 9,000 km radius and lateral damping is removed altogether, a quasi-steady vortex emerges, but the structure of this vortex has many unrealistic features. In this solution, the remaining upper-level Rayleigh damping contributes a major portion of the needed source of cyclonic RAM. In a simulation in which the upper-level damping is removed also, the solution is found to be neither quasi-steady nor realistic.

These findings call into question the realism of long-term, sustained tropical cyclone simulations, which require a sufficiently large source of cyclonic RAM to facilitate the existence of a quasi-steady state.

Keywords: tropical cyclones, steady-state, angular momentum

1. Introduction

Hurricanes are intense, warm-cored, cyclonically-rotating, convectively-driven vortices that form over the tropical oceans. A large fraction of these storms form from pre-existing disturbances in the Inter-Tropical Convergence Zone or monsoon trough, typically within 15 deg latitude of the equator. If conditions are favorable, intensification may be rapid, and storms may last for a week or more. Storms that become particularly intense may remain intense (though not maintaining the same peak intensity or radius of maximum wind) for many days (e.g., Hurricane Ivan 2004). However, storms eventually weaken, sometimes due to their propagation out of the tropics and over cooler sea-surface temperatures, sometimes because of increasing vertical wind shear in their environment, or sometimes because of their encounter with land or with rugged topography associated with island terrain. Certainly, from an observational perspective, one could justifiably regard hurricanes as transient vortices.

Corresponding author: Michael T. Montgomery, mtmontgo@nps.edu

DOI: 10.6057/2019TCRR01.04

Notwithstanding the flow complexities of individual hurricanes, our understanding of these vortices has been influenced strongly by the simple, axisymmetric, steady-state hurricane model described in a pioneering study by Emanuel (1986) (henceforth E86). For almost three decades now, this model has served to underpin many ideas about how hurricanes function and even how they intensify from a small, but finite amplitude cyclonic vortex a few hundred kilometers in diameter (Rotunno and Emanuel 1987; Emanuel 2003; Persing and Montgomery 2003; Emanuel 2004; Smith et al. 2008; Bryan and Rotunno 2009b,a; Bister et al. 2011; Montgomery and Smith 2014). As an example of its far-reaching influences, the E86 theory is still used as a basis for deriving updates to the so-called *a priori* potential intensity (PI) theory (Bryan and Rotunno 2009a; Garner 2015; Frisius and Schönemann 2012) as well as for estimates of the impact of hurricane intensity and structure change due to global change scenarios (Camargo et al. 2014; Emanuel 1988).

Given the prominence of the E86 theory, it is pertinent to consider how to apply a steady state theory to observed

hurricanes or simulated hurricanes. Steady-state refers to a condition, where the time derivative of any dependent variable (X) is zero. In observed and simulated hurricanes, variations in structure over a variety of time scales is generally observed, however. This raises the question whether such vortices are "quasi-steady" realizations of the theoretical steady state hurricane. A broader question is whether "quasi-steady" hurricanes may exist beyond the realm of current theory. It might be possible to construct a quasi-steady state theory based on the requirement that over some suitable time interval Δt, $\frac{\partial}{\partial t}\int_t^{t+\Delta t} X dt' = 0$ for any dependent variable X. One would then time-integrate all of the equations of motion to obtain a system of equations for the time mean of the quasi-steady vortex. Any such quasi-steady theory would need to include covariance terms contributing to the time-mean of all dependent variables. However, the theory presented in E86 is a strict steady-state theory and not a quasi-steady theory as defined above.

Since a hurricane is a system of convective clouds, the convective time scale (~30 min) is one elemental time scale of variability, and an averaging period covering some number, say ten, such periods might provide a suitable average (i.e. 5 hours). The dynamics of the system-scale vortex has other, longer, time scales, e.g., secondary eyewall cycles have a time scale on the order of a day (Willoughby et al. 1982; Abarca and Montgomery 2014; Huang et al. 2012). Brown and Hakim (2013) suggest that inward propagating bands in a long-lived simulated hurricane have a period of five days. By whatever standard, quasi-steadiness requires that there be no trend in all dependent variables on longer time scales.

A further requirement of a quasi-steady hurricane is that it must retain a realistic structure consistent with observations. Otherwise, one should consider the simulated hurricane as *pathological*. The salient features of an observed hurricane are a swirling flow with near-surface wind speed of at least 33 m s^{-1}, with winds generally decreasing with height above the frictional boundary layer, consistent through approximate gradient wind balance with a warm core structure aloft. The more intense hurricanes tend to have an eye that is free of deep clouds. A third salient feature is an in, up and out (or overturning) circulation with strong inflow in the frictional boundary layer, upflow in an approximately circular region of deep clouds forming the eyewall, and a layer of outflow in the upper troposphere. The eyewall slopes outwards with height, with a slope angle on the order of 45 degrees from the horizontal (e.g. Marks et al. 2008, Fig. 3).

Several recent numerical studies have described long-lived simulations of hurricanes in axisymmetric (Hakim 2011; Chavas and Emanuel 2014; Frisius 2015) and three-dimensional (3D) geometries (Brown and Hakim 2013; Camargo et al. 2014; Khairoutdinov and Emanuel 2013; Zhuo et al. 2014). These studies may present candidate models for quasi-steady state hurricanes if 1) the simulation is quasi-steady, as defined above and 2) the simulated hurricane is not pathological as defined above.

A recent study by Smith et al. (2014) has questioned the existence of a realistic globally quasi steady-state hurricane. By global quasi steady state they mean that the macro-scale flow does not vary systematically with time, which is consistent with the definition above. Among other things, echoing Anthes (1982), the Smith et al. study showed that if such a state were to exist, then a source of cyclonic relative angular momentum (RAM) would be necessary to maintain the vortex against the frictional loss of angular momentum at the sea surface. It showed also that while a supply of cyclonic RAM is a necessary condition for a globally steady state hurricane, it is not sufficient (see Smith et al. (2014) for details). It would be necessary also that, above the boundary layer and outside regions where turbulent diffusion is significant, the spin up function S vanish, where S is the dot product of the absolute vorticity vector of the azimuthal mean vortex and the gradient of the diabatic heating rate divided by the potential vorticity of the azimuthal mean vortex (see Smith et al. 2014, sect. 3.2). It would seem to be a logical consequence that, without a steady source of cyclonic RAM, hurricanes must be globally transient, a deduction that accords with observations and with recent month-long, axisymmetric (Schmidt and Smith 2016) and three-dimensional (Kilroy et al. 2016) numerical simulations. In particular, Kilroy et al. show that after reaching a mature stage in a few days, both the inner-core and outer wind field expand with time and the maximum tangential wind slowly declines even in the presence of radiative cooling (cf. Hakim 2011).

In the E86 steady-state hurricane model, cyclonic RAM is assumed to be steadily replenished at large radii in the upper troposphere, but is such an assumption realistic? Even if it were, one might ask: how long does it take to attain this state and does the steady-state vortex predicted by the model bear any relationship to typical observed structures on realistic forecast time scales of a few days? In other models where the vortex is deemed to attain a quasi-steady state, the question arises: what is the source of RAM needed to support this state? To investigate these questions, we present cloud-permitting numerical simulations with putative quasi-steady states, and we investigate whether these are quasi-steady or pathological by the criteria above. In particular, as part of this investigation, we determine the sources of RAM and assess the realism of these sources.

An outline of the remaining paper is as follows. Section 2 reviews briefly the angular momentum requirements needed to support a quasi-steady hurricane on an f-plane. Section 3 presents the numerical model and its configuration. The basic evolutionary characteristics of the cyclonic and anticyclonic portions of the model hurricanes are presented in Section 4. The angular momentum budget for these simulations is analyzed in Section 5. A summary and

discussion of our findings and their relationship to recent work is given in Section 6, where an assessment of some but not all of these published quasi-steady hurricane solutions is given also. The conclusions are given in Section 7.

2. Angular momentum considerations

Before presenting our series of long-time (more than a week or two) cloud-permitting numerical experiments and analyses, it proves useful to review the angular momentum requirement needed to sustain a steady-state hurricane. Although most of this material was presented by Smith et al. (2014), some repetition may both help the reader and facilitate our discussion of the key angular momentum issue examined in this study.

We consider a vertically-aligned, swirling flow on an *f*-plane expressed in cylindrical coordinates (r, λ, z) with corresponding azimuthally-averaged velocity components (u, v, w) and departures therefrom denoted by primes. The azimuthal-mean absolute angular momentum M per unit mass about the vortex axis is defined by the equation:

$$M = rv + \frac{1}{2}fr^2, \tag{1}$$

where f is the Coriolis parameter. Making the anelastic approximation $\rho \approx \rho(z)$, Smith et al. showed that the flux form of the equation for M is:

$$\frac{\partial M}{\partial t} + \frac{1}{r}\frac{\partial ruM}{\partial r} + \frac{1}{\rho}\frac{\partial \rho wM}{\partial z} = E + D, \tag{2}$$

where

$$E = -\frac{1}{r}\langle\frac{\partial ru'M'}{\partial r}\rangle - \frac{1}{\rho}\langle\frac{\partial \rho w'M'}{\partial z}\rangle \tag{3}$$

represents the momentum fluxes associated with asymmetric (eddy) processes, and

$$D = \frac{1}{r}\frac{\partial}{\partial r}\left[r^3 K_r \frac{\partial}{\partial r}\left(\frac{v}{r}\right)\right] + \frac{1}{\rho}\frac{\partial}{\partial z}\left[\rho K_z \frac{\partial M}{\partial z}\right] \tag{4}$$

represents the unresolved horizontal and vertical diffusive processes. Here, the brackets <...> denote an azimuthal average and K_r and K_z are horizontal and vertical eddy diffusivities, respectively. (Note that for simplicity azimuthal variations in eddy diffusivity have been ignored.)

Integrating the steady-state version of (2) over a control volume extending from the axis to $r = R$ and from the surface to $z = H$, and using the boundary conditions that $u = 0$ at $r = 0$, $w = 0$ at $z = 0$ and $z = H$, and $\partial M/\partial z = 0$ (free-slip) at $z = H$, gives

$$\int_0^H [\rho ruM + \langle\rho ru'M'\rangle]_{r=R}dz = -\int_0^R \left[\rho K_z \frac{\partial M}{\partial z}\right]_{z=0} rdr + \int_0^H \left[\rho K_r r^3 \frac{\partial}{\partial r}\left(\frac{v}{r}\right)\right]_{r=R} dz. \tag{5}$$

After vertically integrating the steady-state version of the continuity equation

$$\frac{\partial ru}{\partial r} + \frac{1}{\rho}\frac{\partial \rho rw}{\partial z} = 0 \tag{6}$$

from $z = 0$ to $z = H$, radially integrating this equation from $r = 0$ to $r = R$, and again using the boundary conditions that $u = 0$ at $r = 0$, and $w = 0$ at $z = 0$ and $z = H$, one obtains

$$\int_0^H [\rho ru]_{r=R}dz = 0. \tag{7}$$

It follows trivially that

$$\int_0^H \left[\rho ru\left(\frac{1}{2}fr^2\right)\right]_{r=R} dz = 0, \tag{8}$$

showing that, in a steady state, the vertically-integrated radial influx of planetary angular momentum density must vanish at any radius. The vanishing of this integral is independent of the rate at which the azimuthally-averaged, low-level radial velocity decays with radius. [This observation sharpens the conclusions of Smith et al. (2014) (their footnote on p4)].

For sufficiently large radius R, the relative angular momentum will be small compared to the planetary angular momentum, i.e., $M(R, z) \approx \frac{1}{2}fR^2$. This result, together with (8), implies that

$$\int_0^H [\rho ruM]_{r=R}dz \approx \int_0^H \left[\rho ru\left(\frac{1}{2}fr^2\right)\right]_{r=R} dz = 0. \tag{9}$$

Inserting (9) into (5) then yields the steady-state angular momentum balance of the vortex:

$$\int_0^H [\langle\rho ru'M'\rangle]_{r=R}dz = -\int_0^R \left[\rho K_z \frac{\partial M}{\partial z}\right]_{z=0} rdr + \int_0^H \left[\rho K_r r^3 \frac{\partial}{\partial r}\left(\frac{v}{r}\right)\right]_{r=R} dz \tag{10}$$

valid for sufficiently large radius R and for either axisymmetric or three-dimensional hurricane flows.

From Eq. (10), it is evident that *the planetary angular momentum of the atmosphere has completely dropped out of the angular momentum balance of the vortex.* The

vanishing of the integrated influx of planetary angular momentum into a hurricane is the analogue of the vanishing Coriolis torque across a meridional surface when considering the angular momentum balance of the middle-latitude westerly jet (see, e.g., Lindzen 1990). In other words, the atmosphere's rotation cannot supply net angular momentum to maintain a steady vortex. The only way that the Earth's rotation can enter the angular momentum balance of the vortex is indirectly via the boundary conditions where the swirling flow component, itself, must exhibit special characteristics as discussed below.

According to Eq. (10), the only possible sources of M available to maintain a hurricane in a steady state could be the radial diffusion of cyclonic angular *velocity* at $r = R$ [Note that the quantity that is radially diffused in the tangential momentum equation is the angular velocity, v/r, and *not* the angular momentum.] at heights where the flow is anticyclonic (the second term on the right of Eq. (10)), the vertical diffusion at the ocean surface at radii where the flow is anticyclonic (contained in the first term on the right of Eq. (10)), a positive radial eddy flux of tangential momentum at $r = R$ (through the term $[<\rho ru'M'>_{r=R}]$), or vertical diffusion and/or frictional torque of relative angular momentum arising at the upper boundary of the model (term not written here). The specific source terms of M that arise at the upper boundary using the chosen numerical model are written out explicitly in Section 5.

That the Earth's rotation cannot supply a net radial angular momentum flux to the steady vortex seems to be an under-appreciated result in the hurricane and geophysical fluid dynamics communities. The underlying assumption of many with whom we have spoken seems to be that the ambient rotation of the atmosphere provides an unlimited supply of cyclonic angular momentum. If this assumption was correct, then a plausible explanation of the dynamical elements needed for a steady-state hurricane would be trivial indeed!

Specific contributions to the vortex-scale M-balance (10) will be discussed in Section 5.

3. The Model and experiments

a. Model core

Experiments are performed using the axisymmetric version of the CM1 numerical model, version 16, a non-hydrostatic and fully compressible cloud model (Bryan and Fritsch 2002). [For a complete description of the three-dimensional model and variable definitions see the technical document "The governing equations for CM1", available for download at http://www.mmm.ucar.edu/people/bryan/cm1 and available also from G. Bryan. For a complete description of the axisymmetric version of CM1, see the paper by Bryan and Rotunno (2009b).]

The reference sounding is a nearly moist-neutral sounding generated from the axisymmetric Rotunno and Emanuel (1987) model. The calculations are carried out on an f-plane with the Coriolis parameter $f = 5\times10^{-5}$ s^{-1}, corresponding to 20º N.

b. Radiation physics

The effects of radiation are represented by a cloud-interactive longwave/shortwave scheme, described in the CM1 documentation as the "NASA-Goddard longwave and shortwave scheme" (Chou and Suarez 1994a,b, abbreviated NASA-G where necessary); this scheme is credited to the Advanced Regional Prediction System of the Center for Analysis and Prediction of Storms at the University of Oklahoma.

c. Boundary conditions

The lateral boundary condition in the model is a free-slip, rigid wall. At the top boundary, a Rayleigh damping layer of the form $\partial Q/\partial t = -\alpha Q$ is added above heights of 20 km to mitigate the reflection of internal gravity waves. Here Q is one of $\{u, v, w, \theta'\}$, where $\theta' = \theta - \bar{\theta}(z)$ is the perturbation of potential temperature from the initial basic sounding, and α is defined by

$$\alpha(z) = \begin{cases} 0 & z < 20 \text{ km} \\ \dfrac{1}{A}\left[1 - \cos\left(\pi \dfrac{z - 20 \text{ km}}{25 - 20 \text{ km}}\right)\right] & z \geq 20 \text{ km} \end{cases} \tag{11}$$

Here we take the constant A to have the default value of 300 s (following the similar numerical setup of Persing et al. (2013)).

d. Air-sea interaction

Sea surface temperature is fixed to 299.3 K (26.15 C). The surface exchange coefficients of heat and momentum are taken to be constant in both space and time. The moist enthalpy transfer coefficient C_k is set equal to 1.29×10^{-3}. This value is close to the mean value (1.2×10^{-3}) derived from the Coupled Boundary Layers/Air-Sea Transfer (CBLAST) experiment (Fig. 6 of Black et al. (2007); Fig. 4 of Zhang et al. (2007)), a recent laboratory study (Fig. 1 of Haus et al. (2010)) near and slightly above marginal hurricane wind speeds, and an energy and momentum budget analysis of the lower-tropospheric eyewall region at major hurricane wind speeds (Bell et al. 2012). The drag coefficient is set to be twice the enthalpy exchange coefficient $C_D = 2 \times C_k = 2.58 \times 10^{-3}$, and is close to the estimated mean value of $C_D = 2.4 \times 10^{-3}$ from observations derived from CBLAST for major hurricane wind speeds by Bell et al. (2012).

e. Turbulence parameterization

Subgrid-scale turbulence is represented by choosing option "iturb=3" in the model, which is designed for problems that do not resolve any part of the turbulent Kolmogorov inertial range. This option requires the external specification of the horizontal mixing length l_h = 700 m and the

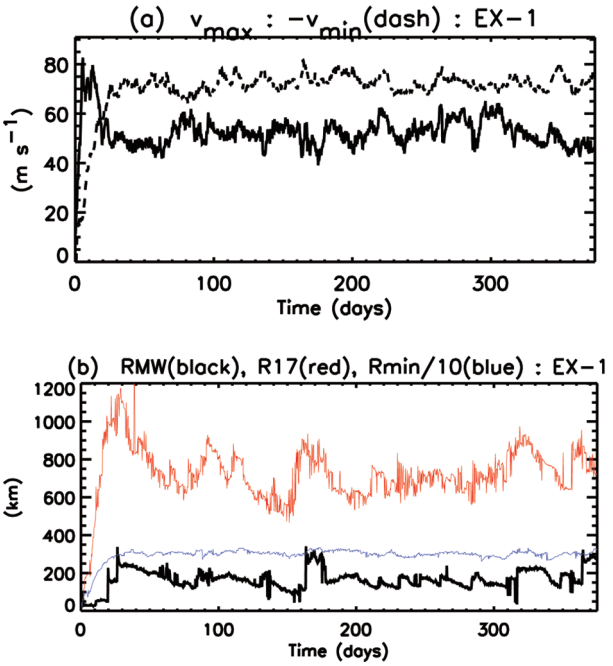

Fig. 1. (a) Maximum (solid) and minimum (dotted) tangential wind from EX-1. (b) Radius of maximum tangential winds (at any height; black), the 2 km height radius of gales (17 m s^{-1}; red), and the radius of minimum tangential winds (at any height; blue) for EX-1.

vertical mixing length far above the surface layer l_∞ = 50 m, which for simplicity are assumed constant in both space and time (Smagorinsky 1963; Lilly 1962). The values chosen for l_h and l_∞ are based on the observational findings of Zhang et al. (2011) and Zhang and Montgomery (2012), and the resulting vertical and horizontal eddy diffusivities that are output in the model simulations. These values are also close to the values recommended by Bryan (2012) in order to produce realistic hurricane structure. Near the bottom boundary the vertical mixing length $l_v = l_v$ (z; l_∞) approaches zero to model a logarithmic surface layer.

f. Precipitation physics

Rainfall is represented here by the NASA-Goddard Cumulus Ensemble Model (Tao and Simpson 1993, NASA-G).

g. Initial conditions

The initial tangential velocity is taken to be in gradient wind balance with a maximum cyclonic velocity of 13 m s^{-1} at the surface at a 100 km radius from the center of circulation. The tangential velocity varies smoothly in space and tends to zero at large radii: it vanishes beyond 400 km radius and above z = 20 km. The initial radial and vertical velocity are set to zero.

As noted above, the numerical simulations presented here employ the axisymmetric configuration of CM1 and adopt a uniform horizontal grid spacing of 3 km and an outer boundary at a radius of 9,000 km. This large outer radius permits the simulated storm to possess a size in which the influence of the outer boundary is minimized (Chavas and Emanuel 2014). In the vertical, there is a stretched grid with 40 grid points between the surface and model top of 25 km; the first grid level is at 25 m altitude and the grid spacing slowly increases with height. The specific model mesh is the same as that described by Persing et al. (2013), Table A1.

h. The experiments

The basic control simulation, EX-1, is as described above, with Rayleigh damping at the top boundary. This simulates a long-lived cyclone that maintains hurricane intensity. We will show below several aspects of the prolonged vortex that are not consistent with known structures of observed hurricanes.

A second experiment, EX-2, is like EX-1, but is without Rayleigh damping. We show below that this simulation exhibits slow but persistent evolution in several quantities, so that it cannot be considered quasi-steady by any standard.

EX-3 is an experiment constructed in the manner of Hakim (2011), with both top-boundary and outer, lateral-boundary Rayleigh damping in a small 1500 km radial domain. We find, like Hakim (2011), that this simulation is quasi-steady, and we show below how damping controls several important aspects of the simulation.

4. Results

We give first a broad summary of the three experiments carried out. In the subsequent section we examine the angular momentum budgets of these experiments.

a. Control experiment – EX-1

Figure 1(a) shows a time series of intensity characterized by the maximum tangential velocity (V_{max}) in EX-1. The vortex intensifies rapidly for about the first 5 days reaching a lifetime maximum of a little over 80 m s^{-1}. The intensity declines after about 15 days and for the remainder of the simulation it remains at hurricane strength, fluctuating about a mean of about 55 m s^{-1}, with large deviations on the order of ±10 m s^{-1}. The figure shows also the magnitude of the minimum tangential velocity ($-V_{min}$), which grows much more slowly than V_{max}, reaching a lifetime maximum of about 75 m s^{-1}, comparable with the lifetime maximum of V_{max}. After about 30 days, $-V_{min}$ fluctuates about an intensity of 80 m s^{-1}, which is appreciably stronger than the intensity of the cyclone for the remainder of the simulation.

Figure 1(b) shows the radius of V_{max} (the RMW), the radius of V_{min} and the radius of gales, the outer radius where the tangential wind equals 17 m s^{-1}. By day 8, the RMW has decreased from the initial value of 100 km to less than 36 km, but exhibits a series of sharp jumps reaching nearly 250 km around 30 days. During the period 100 to

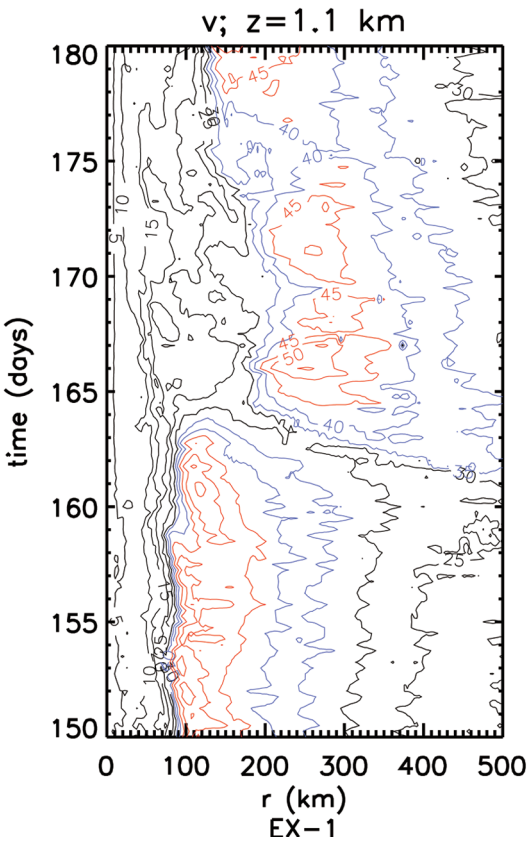

FIG. 2. Mean tangential winds at z = 1 km height in EX-1, plotted radius versus time. The contour interval is 5 m s^{-1}, with black contours between 0 and 30 m s^{-1}, blue contours for 35 and 40 m s^{-1}, and red contours for 45 m s^{-1} and higher.

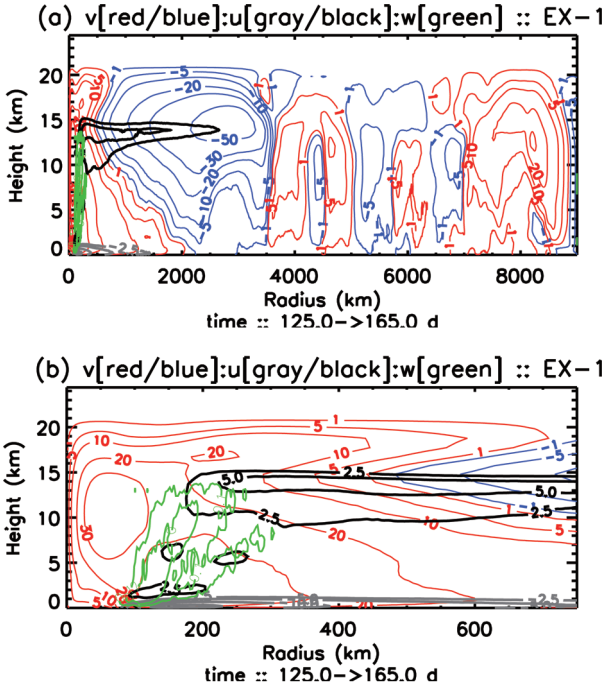

FIG. 3. Radius-height contours of the three components of the wind for EX-1 averaged from 125 to 165 d for a) the complete domain, and b) the innermost 750 km radius. Tangential winds v are shown with the contours ±{1,5,10,20,30,50} m s^{-1} with cyclonic (v > 0) values red, anticyclonic (v < 0) values blue. Radial winds u are shown with the contours ±{2.5,5,10} m s^{-1} with outflow (u > 0) values black, and inflow (u < 0) values gray. Vertical winds w are shown with green contours with values {0.1,0.2} m s^{-1}.

350 days when the cyclone is quasi-steady, the intensity shows considerable variability ranging between 100 and 350 km, which exceeds the largest reported eye size of 160 km radius for Typhoon Carmen (1960; JTWC (1960)). For at least at one such case of variation of the RMW, this resembles a secondary eyewall cycle, with the strongest 1-km height tangential winds (blue and red in Fig. 2) near 110 km radius found to weaken suddenly at 163 days, and a new maximum around 260 km radius near 165 days gradually decreases in radius after that time. This episode of variation of RMW and others found in the simulation will be a topic for future study. The radius of gales varies enormously ranging between 550 and 1150 km. The radius of V_{min} grows progressively for the first 30 days after which it reaches a quasi-steady value of about 3000 km, with little variability compared with the other two radii.

The long-lived vortex in this experiment has a structure that is not consistent with known observations of hurricanes. For example, Fig. 3(a) shows a radius-height cross-section of the tangential wind, time averaged between 125 and 165 days. The intense, primary anticyclone extends from the surface to the tropopause and has a large horizontal extent, reaching to approximately 3500 km radius. During the foregoing time interval, the RMW varies between 120 and 300 km (Fig. 1b) and persistent eyewall convection is found to lie within the same radial range (Fig. 3b). At smaller radii, within the simulated eye, a secondary maximum of tangential winds, of more than 30 m s^{-1} is found at 10 km height, a feature with no known real-life analogue and one that is not a feature of the E86 theory.[1] Large annular cells of cyclonic/anticyclonic winds exist in the far-field environment (r > 4000 km). These cells are not persistent, but align themselves at characteristic radii (Fig. 4), such as the cyclonic winds found near 4000, 6000, and 8000 km and anticyclonic winds near 5000 and 7000 km.

Through a period of quasi-steady cyclonic intensity (150 to 170 h; Fig. 5), the inner-core exhibits much variation in structure. In the upper-level eye, the cyclonic flow described in Fig. 3(b) is depicted by the concentration of M contours (black) near 50 km radius at 150 and 160 days.

[1]The origin of the upper-level tangential wind maximum, namely an annular cyclonic jet contained within the eye, appears to be subtle and complex, but beyond the scope of the present study.

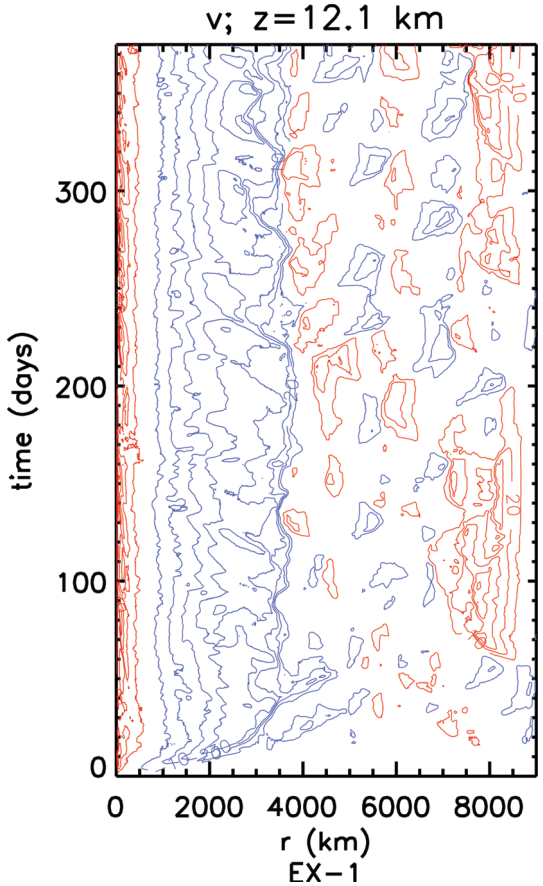

Fig. 4. Mean tangential winds (smoothed in time with a two-day running mean) at z = 12 km height in EX-1, plotted radius versus time. The contour interval is 10 m s^{-1}, with blue contours negative and red contours positive.

The M-contours associated with this feature emanate from just inside the RMW in the boundary layer at approximately 100 km, where the inflow jet (blue, Fig. 5) terminates. The upper-level eye cyclone weakens during this period, reforming near 110 km radius by 170 days. Strong diabatic heating (shaded) shows convective activity near the RMW and at other locations both inside and outside the RMW. At 170 days, the primary eyewall is characterized by an outward-sloping region of strong diabatic heating rate and closely-spaced M contours. This highly slanted structure expands from 220 km radius near the surface to 440 km radius near 9 km height. This slope angle of 6 degrees from the horizontal is much smaller than is ever observed (e.g. Marks et al. 2008).

b. Experiment without Rayleigh damping – EX-2

Figure 6 shows the corresponding curves and fields to Figure 1, but for EX-2 in which there is no Rayleigh damping in the upper troposphere. In comparison with EX-1, both intensity and RMW show more intense, short period oscillations (Fig. 6). Now, the RMW expands gradually throughout the simulation, reaching 175 km at 350 days (Fig. 6b). A least-squares linear fit between 194 and 388 days (the latter half of the simulation period) shows an increase in the RMW of 160 m day^{-1}. In addition, the tangential winds in the model stratosphere continue to evolve (Fig. 7), with an intensifying cyclone near the axis and the development of an anticyclone centered at r = 3000 km. The mechanism for accelerating the statically stable air found above the model tropopause is advection of tangential momentum by small scale wave-like phenomena, presumably by gravity waves. The acceleration of stratospheric winds is evident as early as day 3 (not shown).

Figure 8 shows a radius-height cross-section of the tangential wind, time averaged between 250 and 300 days, which should be compared with Fig. 3(a). In this case, because of the lack of damping, the upper-level cyclonic winds extend from 15 km height to model top (z = 25 km). The upper-level anticyclone extends also to the model top and above 20 km, the anticyclone extends to over 6000 km radius.

Clearly, this simulation cannot be considered quasi-steady by any standard and again, the vortex structure is not consistent with known observations of hurricanes.

c. Reproduction of Hakim (2011) – EX-3

The oft cited study by Hakim (2011) presents simulations of quasi-steady state hurricanes for prolonged periods of hundreds of days. Hakim (2011) applies a damping layer to momentum and potential temperature within 5 km of the model top as in EX-1, and to momentum within 100 km of the outer radius, which is 1500 km in his simulations. The damping layer applied near this radius is reminiscent of that in the E86 model discussed in the Introduction. EX-3 replicates the most-pertinent settings of Hakim (2011)'s simulation. In particular, it employs a relatively small radial domain of 1500 km with Rayleigh damping near both the top and lateral boundaries. With this configuration, we can reproduce the main result from Hakim (2011) of a prolonged hurricane for hundreds of days (see Figure 9).

For the first few days, the vortex intensifies rapidly, with V_{max} reaching approximately 80 m s^{-1}. Thereafter, the intensity declines until approximately 30 d, when V_{max} increases again and becomes quasi-steady with time averaged intensity of approximately 65 m s^{-1}. The intensity fluctuations are on the order of 10 m s^{-1}. The upper anticyclone intensifies steadily, with V_{min} reaching a magnitude of around 30 m s^{-1}, and remains quasi-steady beyond 15 days, with little fluctuation thereafter. In contrast to EX-1 and EX-2, the upper anticyclone remains much weaker compared with the mean intensity of the cyclone. After day 50, the radius of maximum winds (Fig. 9b) shows some variability within a range from 50 to 80 km with episodes where the radius of maximum winds briefly exceeds 100 km. The radius of

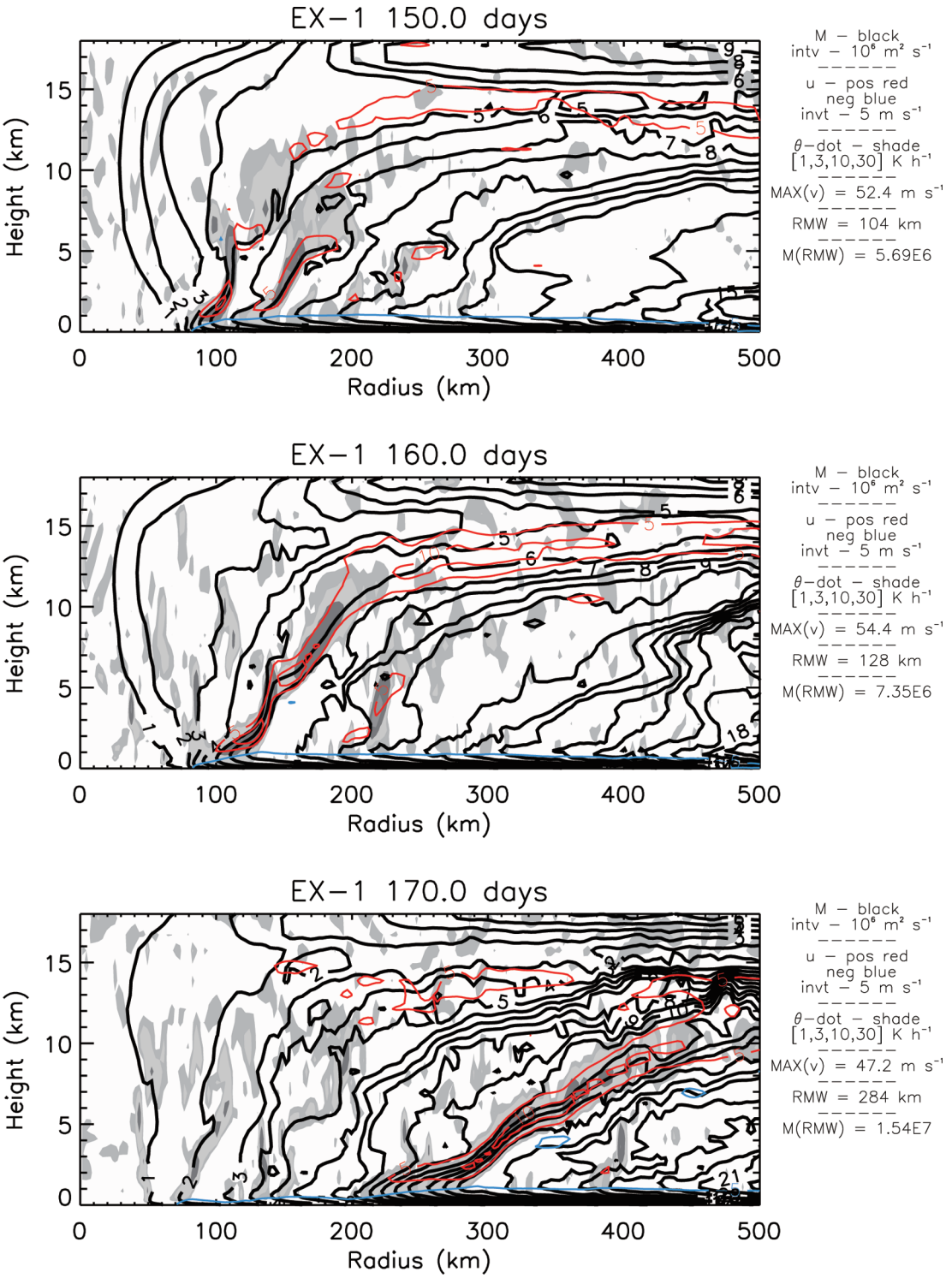

FIG. 5. Plots showing the evolution of the eye/eyewall region in EX-1 at 160, 170, and 180 days. Absolute angular momentum M is shown with black contours of interval 10^6 m^2 s^{-1}. Radial wind u is shown with one blue negative contour $u = -5$ m s^{-1} and with red positive (outflow) contours of interval 5 m s^{-1}. Diabatic heating rate $\dot{\theta}$ is shown by gray shading with levels $\pm\{1,3,10,30\}$ K h^{-1}. Additional information is shown at the right of each panel.

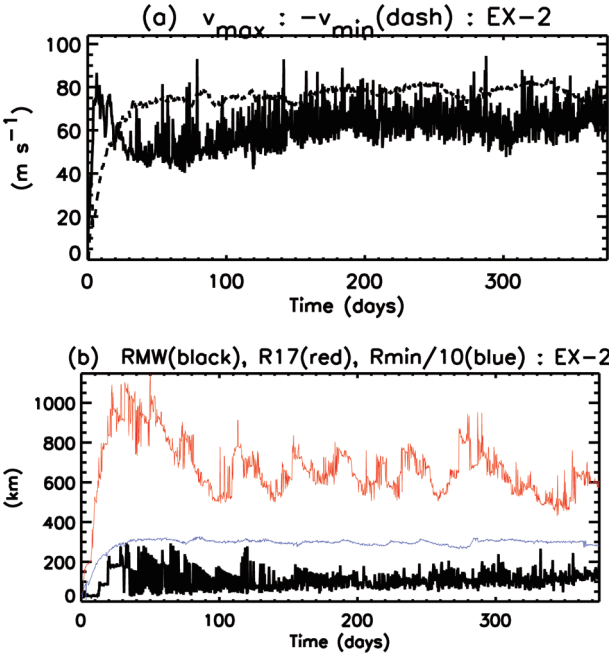

Fig. 6. (a) Maximum (solid) and minimum (dotted) tangential wind from EX-2. (b) Radius of maximum tangential winds (at any height; black), the 2 km height radius of gales (17 m s^{-1}; red), and the radius of minimum tangential winds (at any height; blue) for EX-2.

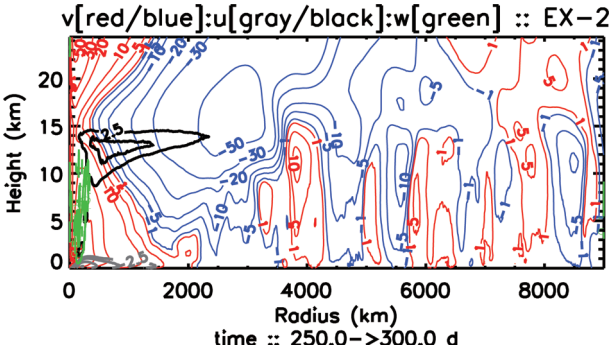

Fig. 8. Radius-height contours of the three components of the wind for EX-2 averaged from 250 to 300 d for the complete domain. Tangential winds v are shown with the contours ±{1,5,10,20,30,50} m s^{-1} with cyclonic ($v > 0$) values red, anticyclonic ($v < 0$) values blue. Radial winds u are shown with the contours ±{2.5,5,10} m s^{-1} with outflow ($u > 0$) values black, and inflow ($u < 0$) values gray. Vertical winds w are shown with green contours with values {0.1,0.2} m s^{-1}.

gales shows a wider range of variability, with minima of 250 km and maxima of 400 km being typical after 50 days. The radius of minimum tangential winds (Fig. 9) is generally very stable at 1400 km, which is also the radius where lateral damping begins. In the larger domain experiment, EX-1, the radius of minimum winds is typically close to

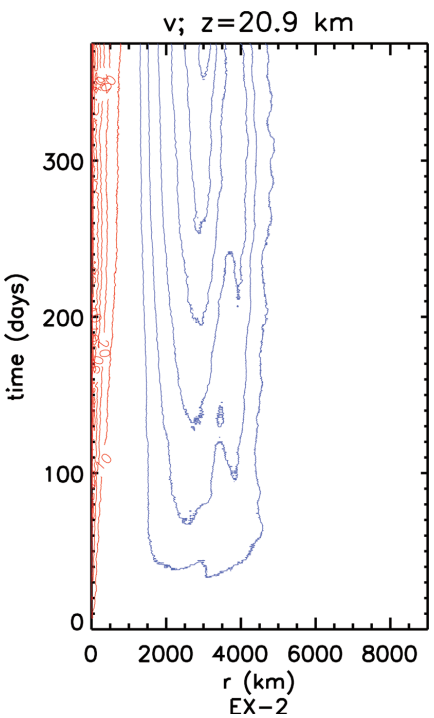

Fig. 7. Mean tangential winds (smoothed in time with a two-day running mean) at $z = 21$ km height in EX-2, plotted radius versus time. The contour interval is 10 m s^{-1}, with blue contours negative and red contours positive.

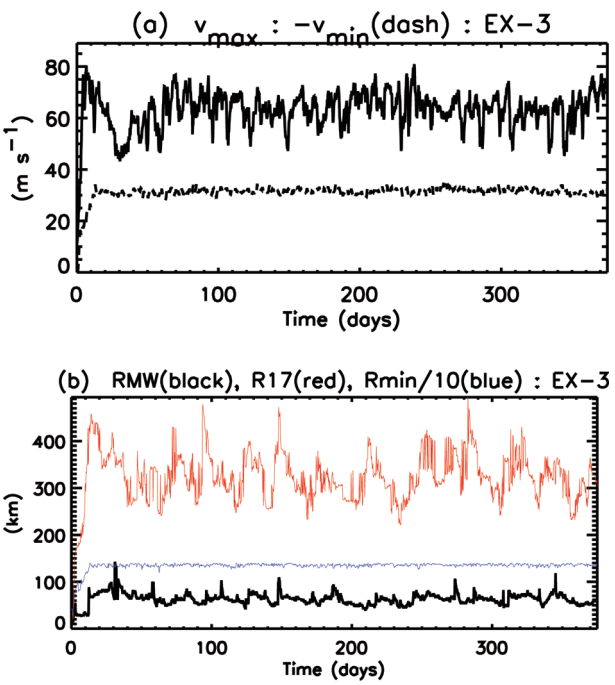

Fig. 9. (a) Maximum (solid) and minimum (dotted) tangential wind from EX-3. (b) Radius of maximum tangential winds (at any height; black), the 2 km height radius of gales (17 m s^{-1}; red), and the radius of minimum tangential winds (at any height; blue) for EX-3.

TABLE 1. *M*-budget summary

Simulation	EX-1	EX-2	EX-3
Analysis interval (d)	$100 < t < 300$	$100 < t < 300$	$100 < t < 300$
R (km)	4001	4001	1496
Tendency $\int \frac{\partial \rho M}{\partial t} r dr dz$			
Mean (kg m^2 s^{-2})	3.79×10^{17}	-1.81×10^{18}	-6.83×10^{14}
Std. Dev (kg m^2 s^{-2})	1.22×10^{19}	2.22×10^{19}	6.12×10^{16}
Lateral flux $-\int \rho r u M dz$			
Mean (kg m^2 s^{-2})	4.04×10^{17}	9.98×10^{17}	5.15×10^{13}
Std. Dev (kg m^2 s^{-2})	9.25×10^{18}	1.36×10^{19}	1.53×10^{15}
Surface drag torque $\int C_D \rho v_{sfc} c_{sfc} r^2 dr$			
Mean (kg m^2 s^{-2})	-1.18×10^{18}	-1.26×10^{18}	-2.49×10^{17}
Std. Dev (kg m^2 s^{-2})	1.38×10^{18}	1.73×10^{18}	4.36×10^{16}
Horizontal diffusion $\int \rho K_r r^3 \frac{\partial v/r}{\partial r} dz$			
Mean (kg m^2 s^{-2})	3.36×10^{15}	4.01×10^{14}	4.08×10^{10}
Std. Dev (kg m^2 s^{-2})	1.90×10^{16}	1.26×10^{16}	6.75×10^{10}
Upper Rayleigh damping $\int \alpha \rho v r^2 dr dz$			
Mean (kg m^2 s^{-2})	5.55×10^{17}	---	-1.55×10^{15}
Std. Dev (kg m^2 s^{-2})	1.31×10^{17}	---	7.26×10^{15}
Lateral Rayleigh damping $\int \alpha \rho v r^2 dr dz$			
Mean (kg m^2 s^{-2})	---	---	2.87×10^{17}
Std. Dev (kg m^2 s^{-2})	---	---	8.18×10^{16}

3500 km. The smaller domain size of EX-3 severely limits the radius of minimum winds.

5. Angular momentum budgets

The absolute angular momentum budget for the extended simulations derived in section 2 are summarized in Table 1. For the budget we apply a time-dependent form of Eq. (5) to the simulations described in section 3h. In addition, we include Rayleigh damping terms near the upper and lateral boundaries. The angular momentum budget integrated over a circular cylinder of radius R and height $H = z_{top}$, the top of the numerical model, is as follows

$$\int_0^H \int_0^R \frac{\partial \rho M}{\partial t} r dr\, dz = \int_0^H [-\rho r u M]_{r=R} dz - \int_0^R C_D \rho v_{sfc} c_{sfc} r^2 dr + \int_0^H \left[\rho K_r r^3 \frac{\partial v/r}{\partial r}\right]_{r=R} dz - \int_0^H \int_0^R \alpha \rho v r^2 dr\, dz - \int_0^H \int_0^R \alpha^\star \rho v r^2 dr\, dz \quad (12)$$

where the term on the left-hand side is the volume-integrated tendency of M. On the right hand side are: the volume integral of the radial flux of M; the integral of the vertical diffusion of angular momentum across the bottom boundary due to surface drag using the surface momentum transfer in the model; the horizontal diffusion of angular velocity integrated over the lateral boundary; the integral of Rayleigh damping in the model stratosphere; and finally the integral of the Rayleigh damping contribution confined to a layer adjacent to the outer lateral boundary, which is used only in EX-3 (see below for definition). Although beyond the scope of the present study, one could modify (12) to apply to quasi-steady situations by integrating through an interval of time; this would force the inclusion of the fluctuating covariance term in the flux across the lateral boundary and a covariance contribution to the surface drag torque. The surface wind speed is denoted by c_{sfc}, and surface tangential winds by v_{sfc}. Quantities involving c_{sfc} and v_{sfc} use the surface (log-) layer extrapolation scheme to estimate the 10-m wind. [In reference to version 16 of CM1, selection of parameters to suppress Rayleigh damping at the top boundary (`irdamp=0') and with no-slip top and bottom boundary condition (`bcuturbu=3', required for bulk aerodynamic surface formula) leads to an erroneous stress term at the top boundary. In the results presented here, this

error has been corrected.]

The damping function for the stratospheric damping layer α is defined by (11). The additional lateral Rayleigh damping function used in EX-3 is given by the formula:

$$\alpha^{\star}(r) = \begin{cases} 0 & r < 1400 \text{ km} \\ \frac{1}{A}\left[1 - \cos\left(\pi \frac{r - 1400 \text{ km}}{1500 - 1400 \text{ km}}\right)\right] & r \geq 1400 \text{ km} \end{cases} \quad (13)$$

which applies damping on all three velocity components to a state of rest in a radial band 1400 < r ≤ 1500 km; the potential temperature perturbation θ' is similarly damped.

Table 1 shows a sample mean and sample standard deviation of *M*-budget terms averaged between 100 and 300 days for the three experiments.

Experiment EX-1 (Fig. 1a) shows a prolonged and quasi-steady intensity after 100 days. During this extended interval, the *M*-tendency term and the mean radial influx of *M* (Fig. 10a, red and blue curves, respectively), have the largest magnitudes. However, from Table 1, these two terms nearly cancel (the means of these quantities are nearly two orders of magnitude smaller than the corresponding standard deviation over the quasi-steady averaging period).

Because of the large temporal variability shown in the *M*-budget calculations and the coarse (six-hourly) temporal sampling of the output, a statistical interpretation of the budget results is presented. Overall, the spin-down tendency from the surface drag term (black curve, Fig. 10a) is about twice the magnitude of the spin-up tendency due to Rayleigh damping in the model stratosphere (blue dotted curve, Fig. 10b; and column for EX-1 in Table 1). The spin-up torque represented by the upper-level Rayleigh damping is the numerical device used to control the reflection of gravity waves off of the rigid top boundary. In this case, the damping layer acts upon the outflow anticyclone, which abuts the stratosphere and reduces the strength of the upper anticyclone. Of course, there is no real-life analogue for this Rayleigh damping of momentum, which is introduced merely as a numerical expedient.

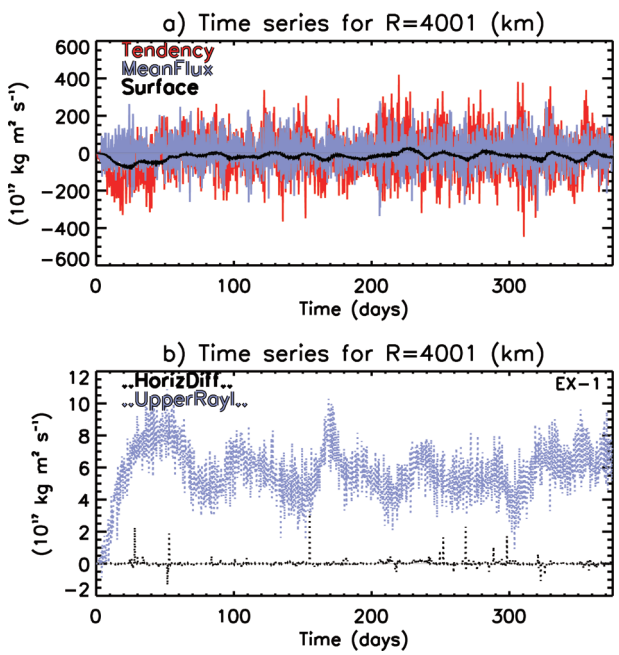

Fig. 10. Terms of the angular momentum budget (Eq. 12) computed for EX-1 inside an integration cylinder of radius *R* = 4001 km. Two panels are used for clarity. The terms represented are, referring to corresponding terms of Table 1: 1) "Tendency" red solid, 2) "MeanFlux", the lateral flux, blue solid, 3) "Surface", the surface drag torque, black solid, 4) "UpperRayl.", the upper Rayleigh damping, blue dotted, and 5) "HorizDiff", the horizontal diffusion, black dotted.

In EX-2, without Rayleigh damping, the surface drag torque is somewhat larger in magnitude within the analysis region of *R* = 4000 km (Table 1). However, there remains a source for *M* as a result of surface torque at greater radii (see Section 5a below). The radial flux and tendency terms are of greater magnitude also than the corresponding terms in EX-1, but the mean of these terms is much less than the standard deviation of these terms. The changes in the mean value of *M* within the analysis region are consistent with the negative surface drag torque. However, there is a larger influx of *M* entering the 4,000 km radius analysis cylinder than the corresponding influx calculated for EX-1. The question then is what is the source of this influx? The only possible source could be from an anticyclonic surface torque beyond the 4,000 km radius cylinder.

a. Net Surface Torque (NST)

The important role of the surface anticyclone is that it enables the diffusion of cyclonic *M* from the lower boundary into the fluid and thereby opposes, in part, the loss of RAM beneath the cyclonic part of the flow. From Eq. (12), the net surface drag torque (NST) at the lower surface integrated from the axis to a radius *R* is given by

$$\mathrm{NST}(R) = -\int_0^R C_{\mathrm{D}} \rho v_{\mathrm{sfc}} c_{\mathrm{sfc}} r^2 dr. \quad (14)$$

The RAM source associated with the surface winds inside *R* = 4000 km is shown for EX-1 in Fig. 10(a). The net surface torque is mostly negative, but occasionally positive during the quasi-steady period. To gain further insight into the radial structure of NST for EX-1, Figure 11 shows a radius-time Hovmoeller plot of NST presented as a function of integrating radius *R* and time. After a time of 100 days, Fig. 11 suggests that this term is not able to consistently counter the loss of angular momentum associated with the drag term under the strong cyclonic wind region. The temporal and spatial variability shown in NST for *R* > 4000 km reflects the inherent unsteadiness of the surface drag torque. Clearly, the NST associated with the interaction of

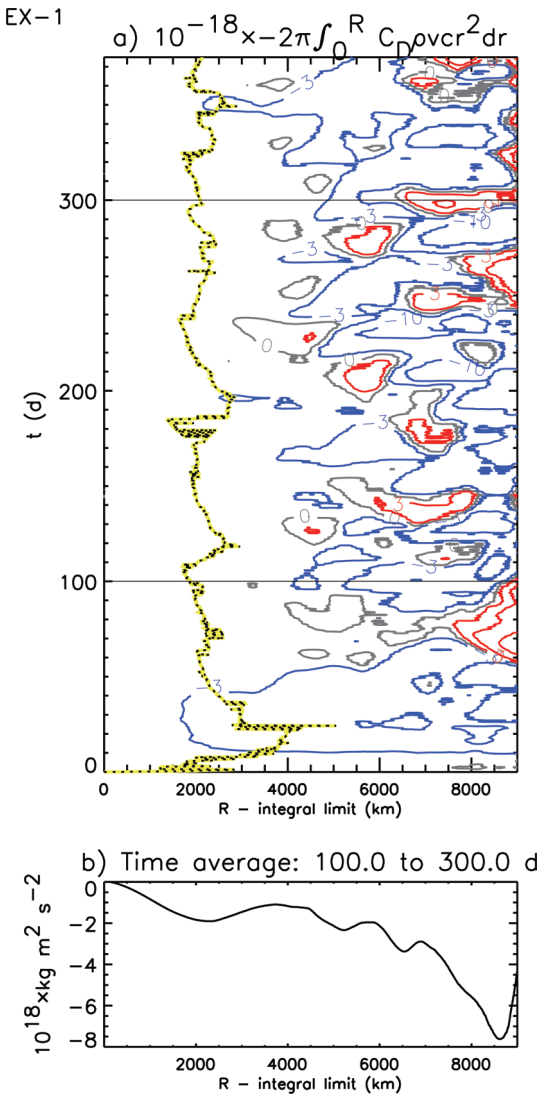

FIG. 11. a) Contour plot of the radial integral of the drag torque (normalized by 10^{18}) plotted as a function of integrating radius R and time from EX-1. Blue contours are negative, gray is zero, and red are positive (i.e., a positive tendency for integrated M), with contour values $\pm\{3,10,30,100\}$ kg m^2 s^{-2}. The black-and-yellow spotted line is the radius r_0 where the tangential winds first vanish at the surface beyond the RMW. b) The time-averaged radial integral of drag torque averaged between 100 and 300 days (as shown by black horizontal lines in the top panel.)

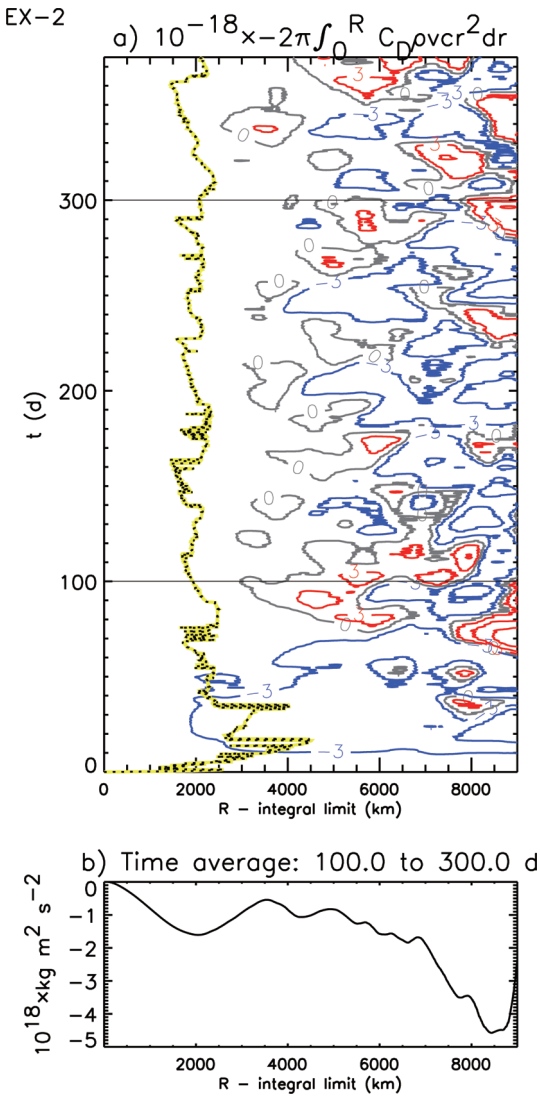

FIG. 12. a) Contour plot of the radial integral of the drag torque (normalized by 10^{18}) plotted as a function of integrating radius R and time from EX-2. Blue contours are negative, gray is zero, and red are positive (i.e., a positive tendency for integrated M), with contour values $\pm\{3,10,30,100\}$ kg m^2 s^{-2}. The black-and-yellow spotted line is the radius r_0 where the tangential winds first vanish at the surface beyond the RMW. b) The time-averaged radial integral of drag torque averaged between 100 and 300 days (as shown by black horizontal lines in the top panel.)

the primary anticyclone (r < 3500 km) with the surface is not enough to overcome the loss of RAM associated with the primary cyclone.

Figure 12 shows the corresponding NST as a function of integrating radius R and time for EX-2. In this simulation, which has no Rayleigh damping, there is a somewhat greater preponderance of positive NST values in comparison to EX-1. These positive values are evidenced by the somewhat greater extent of the gray zero contour and the smaller-in-value negative temporal averages (Note the change in ranges of values between Figs. 11b and 12b). Without Rayleigh damping at the top boundary in EX-2, the surface drag torque at large radii offsets more of the negative tendency than in EX-1.

Figure 13 compares a time series of NST(R = 9000 km) (implicit in Figure 12a) with one for the domain-integrated tendency of M (and RAM) as given by the left-hand side of Eq. (12) for a cylinder of radius R = 9000 km (NMT in the

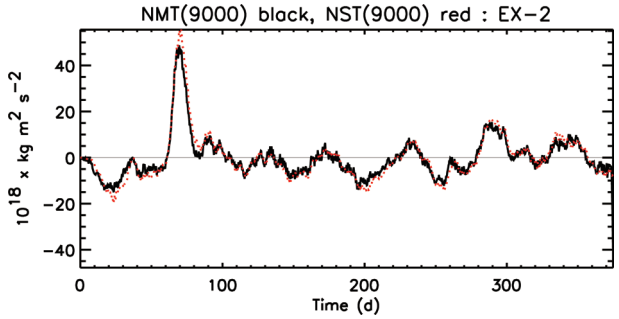

FIG. 13. Time series of the domain integrated tendency of absolute angular momentum (NMT, black solid) and domain integrated surface drag torque (NST, red dotted) for EX-2.

figure). While both curves show significant fluctuations with time, the NST curve tracks the tendency term very closely. This result affirms the important constraint of the domain drag torque on the system evolution as predicted by Smith et al. (2014).

b. Relationship of EX-2 to Chavas and Emanuel (2014)

Chavas and Emanuel (2014) presented long-running, axisymmetric hurricane simulations in a large radial domain (12,288 km) using the CM1 model with Rayleigh damping on horizontal momentum fields near and above the model tropopause. They presented an "equilibrium" solution by evaluation of the low-level tangential wind field, determined that simulation to be in a quasi-steady state, and estimated the radius as which NST vanishes, r_τ, as approximately 2400 km. At r_τ, there is sufficient cyclonic torque beneath the surface anticyclone to offset the accumulated anticyclonic torque beneath the hurricane. The temporal variability in the far-field in EX-2 shown by Figs. 12 and 13 provides an opportunity to evaluate in detail r_τ and the possible quasi-steadiness of the surface drag torque.

Figure 14 shows for EX-2 that between 100 and 300 days, r_τ is defined 97% of the time with an average value of 4300 km and ranges between 2680 and 8980 km. Having identified a mean value of r_τ, Fig. 12(b) shows, however, that NST(4300 km) < 0. Thus, mean r_τ would not suffice to characterize the time-averaged radial distribution of surface drag torque. Indeed, Fig. 12(b) suggests that for this averaging period there is no appropriate value for r_τ: on average, for radii r > 4300 km, NST becomes further negative until the outer boundary, where a standing anticyclone (see Fig. 8 at 9000 km radius) at the outer boundary finally brings NST to a near-zero value (Fig. 13). The outer-boundary anticyclone, an unsteady feature resulting from the large, yet still limited domain size, serves finally as the torque-restoration mechanism for the complete domain.

In the E86 theory, the far-field radius where the near-surface tangential wind vanishes is defined as r_0. This theory assumes that the tangential winds vanish identically outside of this radius. In the numerical experiments EX-1 and EX-2, the tangential winds become alternately anticyclonic and cyclonic beyond the first radius of vanishing tangential wind. For these experiments, we continue to denote r_0 as the first radius at which the tangential wind vanishes. Average values for r_0 from the EX-1 and EX-2 simulations (Figs. 11, 12, 14) are about 2000 km, much larger than the 400 km value infered from observations by Chavas and Emanuel (2010).

Elementary considerations imply that r_0 can never be as large as r_τ, namely $r_0 < r_\tau$. Therefore, in the absence of a

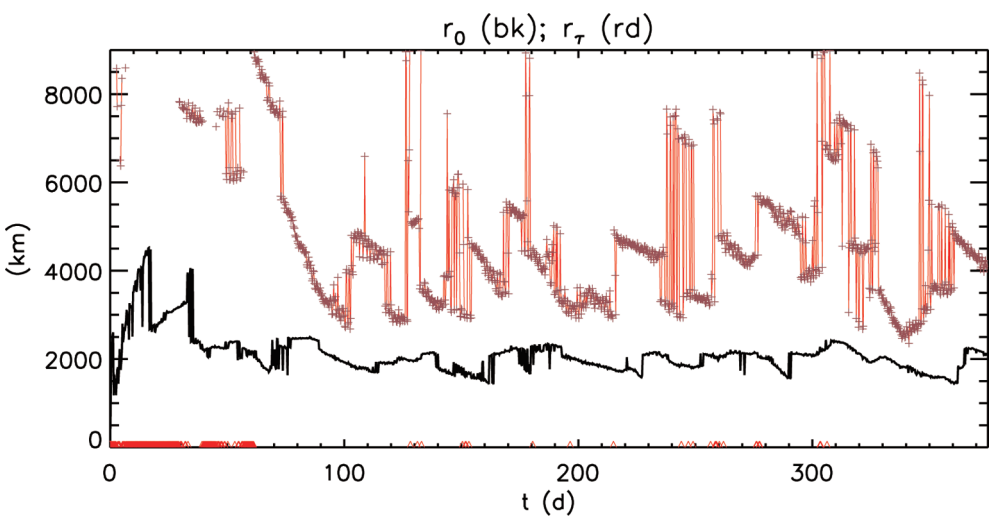

FIG. 14. Time series of the radius of vanishing tangential winds r_0 (black) and radius of vanishing surface drag torque r_τ (red). Data are displayed with a six-hour spacing. The quantity r_τ is shown by '+' when defined, and by a triangle along the bottom of the display when not defined.

source of cyclonic RAM in the upper atmosphere (associated with presumed synoptic-scale eddy angular momentum fluxes [not present in these axisymmetric experiments]), the E86 theory is unable to provide a pathway for ultimately restoring the RAM lost in the domain.

In contrast to E86, Chavas and Emanuel (2014) show anticyclonic surface winds outside of r_0, and, consistent with Smith et al. (2014), invoke the diffusion of the earth's cyclonic angular momentum between r_0 and r_τ as sufficient to balance the angular momentum lost beneath the cyclonic part of the hurricane. Without Rayleigh damping in the stratosphere, the EX-2 solution closely follows such a conceptual framework, but it should be noted that EX-1 more closely models the experimental configuration of Chavas and Emanuel (2014) with the inclusion of a stratospheric damping layer. [Table 1 identifies the upper Rayleigh damping as a significant source of cyclonic RAM in EX-1. A similar analysis to Fig. 14 for EX-1 (not shown) finds that r_τ is more-frequently undefined after 100 days than in EX-2.]

c. Relationship of EX-3 to Hakim (2011)

As noted in Smith et al. (2014), inspection of Hakim's Fig. 5 suggests that it is near the outer boundary where much of the cyclonic RAM is restored, typically between heights of 5 and 7 km where air parcels cross a large gradient in the M-surfaces as they descend in that region.

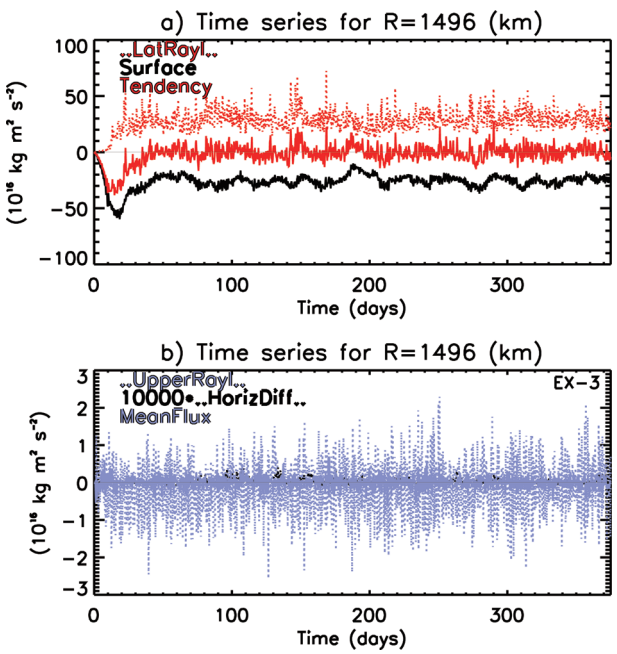

FIG 15. Terms of the angular momentum budget (Eq. 12) computed for EX-3 inside an integration cylinder of radius R = 1496 km. Two panels are used for clarity. The terms represented are, referring to corresponding terms of Table 1: 1) "LatRayl", the lateral Rayleigh damping, red dotted, 2) "Surface", the surface drag torque, black solid, 3) "Tendency", red dotted, 4) "UpperRayl", the upper Rayleigh damping, blue dotted, 5) "HorizDiff", the horizontal diffusion, shown with a multiplier to improve depiction, black dotted, and 6) "MeanFlux", the lateral flux, blue solid.

To further test our hypothesis on the important role artificial sources of RAM can play in supporting long-lived model hurricanes, we examine the M budget for our simulation that replicates Hakim's control experiment. Shown in Fig. 15 is the angular momentum budget Eq. (12), except that an additional term for the Rayleigh damping near the lateral boundary has now been added. Comparing the relative importance of terms in Table 1 for EX-3 and EX-1, we see that the new lateral damping term replaces the role of the upper damping term as the principal source term of RAM, offsetting the loss of RAM due to surface friction in the primary cyclone.

In retrospect, EX-1 can be viewed as a large-domain version of EX-3, since an analogue of EX-3 with lateral damping would present a damping zone more than twice the radial extent (4000 km) of the anticyclonic circulation. One could think of the lateral damping as representing processes at large radii (r > 1500 km) that offset the loss of angular momentum due to friction in the cyclone. However, the only realistic process to achieve this replenishment of M would be surface friction beneath a complimentary anticyclone. As noted in section 4, EX-1 does show an anticyclone with an intensity much greater than that found in EX-3 (compare Figs. 1a and 9a), but the anticyclonic circulation is most intense aloft, more readily able to access the artificial source of RAM in the stratosphere. The intensity of the cyclone is stronger in EX-3 than in EX-1, suggestive of the role that an artificial source of RAM closer to the cyclonic circulation might have on various measures of intensity. These experiments highlight a sensitivity of the simulations to the nature of angular momentum sources.

EX-3 demonstrates the dominant role of artificial momentum sources in determining the structure of the quasi steady-state. Compared to EX-1, the use of a stronger momentum damping term in the form of lateral damping (see Table 1) produces a more "realistic-looking" anticyclone with intensity of just 30 m s^{-1}.

These findings suggest that Hakim's interpretation that the radiative cooling is the critical factor permitting prolonged, quasi-steady simulations may be applicable only when a large, artificial source of angular momentum is available.

6. Summary and discussion

Despite the fact that we have presented only three prototype calculations, there would appear to be significant ramifications of our finding that, for the two solutions with quasi-steady cyclones (EX-1 and EX-3), the sources of cyclonic RAM are artificial and/or display an intermittent torque at the ocean surface at large radii. The case without artificial damping (EX-2) did not become quasi-steady by any standard. These findings support those of Smith et al.

(2014). In particular, the results illustrate the well-known fact that simulated storms growing in a favorable kinematic and thermodynamic environment reach a steady or quasi-steady state in a time of a few days as characterized by the maximum tangential wind, V_{max}, does not mean that these storms are globally quasi steady. These results are a reminder that merely using V_{max} is not sufficient for assessing global quasi-steadiness. A new finding here is that the radius of minimum anticyclonic winds at upper levels appears to exhibit the least variability of the metrics of storm structure.

Concerns regarding the realism of the 400 plus day axisymmetric hurricane simulations of Hakim (2011) were expressed by Smith et al. (2014), who pointed out in particular that the lateral Rayleigh damping towards a zero wind field used in his model must provide the needed RAM to sustain the hurricane. In the three-dimensional extension of the Hakim (2011) study, Brown and Hakim (2013) used the CM1 model, but with a closed domain boundary condition and with a zone of Rayleigh damping of the wind field towards zero. According to these authors (Brown and Hakim 2013, p. 1808), this type of boundary forcing "... provides a constant source of angular momentum, which is needed to maintain equilibrium, since air parcels lose angular momentum on inflow and conserve angular momentum on outflow as they circulate the closed domain." Specifically, this lateral Rayleigh damping at such a radius has the effect of *controlling* the most significant phenomenological challenge in trying to construct a quasi-steady state hurricane simulation, by reducing the intensity and spatial scale of the primary anticyclone. In this paper, we demonstrated the crucial role of the lateral damping in supplying the needed cyclonic RAM to maintain the simulated hurricane in this configuration.

Recently, Frisius (2015) presented long-time sustained hurricane simulations in axisymmetric geometry using a modified HURMOD model. The HURMOD is a hurricane model described in Frisius and Wacker (2007), but in Frisius (2015) a simplified, axisymmetric version is used. The model features a strong damping of moisture fields in the environment, which is designed to "avoid excessive moistening of the far-field" that spawns convection; the far-field convection "interferes with the TC [tropical cyclone] in the axisymmetric model" (Frisius 2015, Sec. 2.3).

Frisius (2015) shows that when a Rayleigh damping layer is included at upper levels in the model, the damping provides a crucial source of cyclonic RAM, while removing the damping layer forces the needed source of cyclonic RAM to the lower surface under a relatively strong anticyclone.

As discussed in section 5b, Chavas and Emanuel (2014) presented also long-time sustained hurricane solutions using the CM1 model in an axisymmetric configuration. Like Hakim (2011), Chavas and Emanuel's formulation included lateral damping, but the lateral source of RAM was minimized by placing the lateral boundary at a radius of 12,288 km. Although Chavas and Emanuel noted the limitations of their findings because of the long-time required to achieve the equilibrium regime and the unlikelihood of observing quasi-steady hurricanes in reality over a several day period, they did consider the primary source of RAM in one of their solutions. They reported (but did not show) a surface torque balance that managed to maintain the vortex via the replenishment of RAM by vertical diffusion at the surface in the anticyclonic portion of the outer vortex, as predicted by Smith et al. (2014). However, questions were raised in section 5b about the specifics of their findings as well as their generality. Furthermore, their calculations included the artificial RAM source associated with Rayleigh damping in the upper atmosphere.

Perpetual hurricanes have been found to exist also in three-dimensional doubly-periodic rectangular domains. These solutions exhibit one or more sustained storms for 20 or more days (Khairoutdinov and Emanuel 2013; Zhuo et al. 2014). These solutions do not impose artificial lateral damping and thus do not have this as a source of RAM. While these solutions appear to be plausible sustained hurricanes, it is nonetheless true that the theoretical considerations of Smith et al. (2014) (and in Section 2 herein) should still provide a means of identifying where the source of cyclonic RAM must originate for each individual hurricane to maintain itself. However, the needed source of cyclonic RAM to sustain prolonged cyclonic storms was not investigated by these latter authors and the question pertaining to the precise sources of RAM in their solutions remains unanswered.

Based on the results presented here, the inability to simulate a quasi-steady hurricane without introducing an artificial source of RAM raises concerns about the tenability of steady-state theories for the potential intensity of hurricanes.

7. Conclusions

We have revisited the possibility of obtaining long-term, quasi-steady simulations of tropical cyclones using a state-of-the-art numerical model that incorporates the most recent observational guidance for subgrid scale parameters and air-sea exchange coefficients of heat and momentum. These simulations require either the inclusion of artificial sources of cyclonic relative angular momentum that are numerical expedients with no real-life analogue or a positive surface torque where the near-surface flow is anticyclonic at large radius. In all three simulations presented, the long-term vortex structure was found to be unrealistic in relation to observed tropical cyclones. Of these simulations, the one without lateral and upper-level damping was not quasi steady.

While further simulations would be desirable to test the robustness of the foregoing results, the current results do call into question the physical relevance of globally-steady models for tropical cyclones.

Acknowledgements

JP and MTM acknowledge the support of NSF grant IAA-1313948, and NASA grants NNH09AK561 and NNG09HG031. RKS was supported in part by Grant SM 30/23-1 from the German Research Council (DFG) and by the Office of Naval Research Global under Grant N62909-15-1-N021. The views expressed herein are those of the authors and do not represent sponsoring agencies or institutions. The data used in this paper can be accessed by emailing the corresponding author at: mtmontgo@nps.edu.

References

Abarca, S. F. and M. T. Montgomery, 2014: Are eyewall replacement cycles governed largely by axisymmetric balance dynamics? *J. Atmos. Sci.*, **72**, 82--87.

Anthes, R. A., 1982: *Tropical cyclones: Their evolution, structure, and effects*. Meteor. Monogro. No. 41, Amer. Meteor. Soc., pp 208.

Bell, M. M., M. T. Montgomery, and W. C. Lee, 2012: An axisymmetric view of concentric eyewall evolution in Hurricane Rita (2005). *J. Atmos. Sci.*, **69**, 2414--2432.

Bister, M., N. Renno, O. Pauluis, and K. Emanuel, 2011: Comment on Makarieva et al. 'A critique of some modern applications of the Carnot heat engine concept: The dissipative heat engine cannot exist.' *Proc. R. Soc. A.*, **467**, 1--6.

Black, P. G., E. A. D'Asaro, T. B. Sanford, W. M. Drennan, J. A. Zhang, J. R. French, P. P. Niiler, E. J. Terrill, and E. J. Walsh, 2007: Air-sea exchange in hurricanes: Synthesis of observations from the coupled boundary layer air-sea transfer experiment. *Bull. Amer. Meteorol. Soc.*, **88**, 357--374.

Brown, B. R. and G. J. Hakim, 2013: Variability and predictability of a three-dimensional hurricane. *J. Atmos. Sci.*, **70**, 1806--1820.

Bryan, G. H. and J. M. Fritsch, 2002: A benchmark simulation for moist non-hydrostatic numerical model. *Mon. Wea. Rev.*, **130**, 2917--2928.

Bryan, G. H. and R. Rotunno, 2009a: Evaluation of an analytical model for the maximum intensity of tropical cyclones. *J. Atmos. Sci.*, **66**, 3042--3060.

--- 2009b: The influence of near-surface, high entropy air in hurricane eyes on maximum hurricane intensity. *J. Atmos. Sci.*, **66**, 148--158.

Camargo, S. J., M. K. Tippett, A. H. Sobel, G. A. Vecchi, and M. Zhao, 2014: Testing the performance of tropical cyclone genesis indices in future climates using the hiram model. *J. Climate*, **27**, 9171--9196, DOI:10.1175/JCLI-D-13-00505.1.

Chavas, D. R. and K. A. Emanuel, 2010: A QuikSCAT climatology of tropical cyclone size. *Geo. Res. Letts.*, **37**, DOI:10.1029/2010GL044558.

Chavas, D. R. and K. A. Emanuel, 2014: Equilibrium tropical cyclone size in an idealized state of radiative-convective equilibrium. *J. Atmos. Sci.*, **71**, 1663--1680.

Chou, M. D. and M. J. Suarez, 1994a: *An efficient thermal infrared radiation parameterization for use in general circulation models*. Technical Memorandum 3, Technical Report Series on Global Modeling and Data Assimilation, NASA Tech. Rep. TM-1994-104606, Goddard Space Flight Center, Greenbelt, MD, USA.

--- 1994b: *A solar radiation parameterization (CLIRAD-SW) developed at Goddard Climate and Radiation Branch for Atmospheric Studies*. Technical Memorandum 15, Technical Report Series on Global Modeling and Data Assimilation, NASA Tech. Rep. TM-1999-104606, NASA Goddard Space Flight Center, Greenbelt, MD, USA.

Emanuel, K. A., 1986: An air-sea interaction theory for tropical cyclones. Part I: Steady state maintenance. *J. Atmos. Sci.*, **43**, 585--604.

--- 1988: The maximum intensity of hurricanes. *J. Atmos. Sci.*, **45**, 1143--1155.

--- 2003: Tropical cyclones. *Annu. Rev. Earth Planet. Sci.*, **31**, 75--104.

--- 2004: Tropical cyclone energetics and structure. *Atmospheric Turbulence and Mesoscale Meteorology*, E. Fedorovich, R. Rotunno, and B. Stevens, eds., Cambridge University Press, Cambridge.

Frisius, T., 2015: What controls the size of a tropical cyclone? Investigations with an axisymmetric model. *Q. J. R. Meteorol. Soc.*, DOI:10.1002/qj.2537.

Frisius, T. and D. Schönemann, 2012: An extended model for the potential intensity of tropical cyclones. *J. Atmos. Sci.*, **69**, 641--661.

Frisius, T. and U. Wacker, 2007: *Das massenkonsistente axialsymmetrische Wolkenmodell HURMOD*. Wissenschaftliche Dokumentation DWD, Offenbach am Main, Germany.

Garner, S., 2015: The relationship between hurricane potential intensity and CAPE. *J. Atmos. Sci.*, **72**, 141--163.

Hakim, G. J., 2011: The mean state of axisymmetric hurricanes in statistical equilibrium. *J. Atmos. Sci.*, **37**, 515--533.

Haus, B. K., D. Jeong, M. A. Donelan, and J. A. Zhang, 2010: Relative rate of sea-air heat transfer and frictional drag in very high winds. *Geophys. Res. Lett.*, **37**, l07802, DOI:10.1029/2009GL042206.

Huang, Y.-H., M. T. Montgomery, and C.-C. Wu, 2012: Concentric eyewall formation in Typhoon Sinlaku (2008) - Part II: Axisymmetric dynamical processes. *J. Atmos. Sci.*, **69**, 662--674.

Joint Typhoon Warning Center, 1960: 1960 Annual Tropical Cyclone Report, pp. 219.

Khairoutdinov, M. and K. Emanuel, 2013: Rotating radiative-convective equilibrium simulated by a cloud-resolving model. *J. Adv. Modeling Earth Sys.*, **5**, 816--825, doi:10.1002/2013MS000253.

Kilroy, G., R. K. Smith, and M. T. Montgomery, 2016: Why do tropical cyclones grow progressively in size and decay in intensity after reaching maturity? *J. Atmos. Sci.*, **73**, 487--503.

Lilly, D. K., 1962: On the numerical simulation of buoyant convection. *Tellus*, **14**, 148--172.

Lindzen, R. A., 1990: *Dynamics in Atmospheric Physics*. Cambridge University Press, Cambridge.

Marks, F. D., P. G. Black, M. T. Montgomery, and R. W. Burpee, 2008: Structure of the eye and eyewall of Hurricane Hugo (1989). *Mon. Wea. Rev.*, **136**, 1237--1259.

Montgomery, M. T. and R. K. Smith, 2014: Paradigms for tropical cyclone intensification. *Aust. Meteor. Ocean. J.*, **64**, 37--66.

Persing, J. and M. T. Montgomery, 2003: Hurricane superintensity. *J. Atmos. Sci.*, **60**, 2349--2371.

Persing, J., M. T. Montgomery, J. C. McWilliams, and R. K. Smith, 2013: Asymmetric and axisymmetric dynamics of tropical cyclones. *Atmos. Chem. Phys.*, **13**, 12299--12341.

Rotunno, R. and K. A. Emanuel, 1987: An air-sea interaction theory for tropical cyclones. Part II: Evolutionary study using a nonhydrostatic axisymmetric numerical model. *J. Atmos. Sci.*, **44**, 542--561.

Schmidt, C. W. and R. K. Smith, 2016: Tropical cyclone evolution in a minimal axisymmetric model revisited. *Q. J. R. Meteorol. Soc.*, **91**, 99--164.

Smagorinsky, J., 1963: General circulation experiments with the primitive equations. I: The basic experiment. *Mon. Wea. Rev.*, **91**, 99--164.

Smith, R. K., M. T. Montgomery, and J. Persing, 2014: On steady-state tropical cyclones. *Quart. J. Roy. Meteor. Soc.*,

DOI:10.1002/qj.2329.

Smith, R. K., M. T. Montgomery, and S. Vogl, 2008: A critique of Emanuel's hurricane model and potential intensity theory. *Quart. J. Roy. Meteor. Soc.*, **134**, 551--561.

Tao, W. K. and J. Simpson, 1993: Goddard cumulus ensemble model. Part I: Model description. *Terr. Atmos. Oceanic Sci.*, **4**, 35--72.

Willoughby, H. E., J. A. Clos, and M. G. Shoreibah, 1982: Concentric eye walls, secondary wind maxima, and the evolution of the hurricane vortex. *J. Atmos. Sci.*, **39**, 395--411.

Zhang, J. A., W. M. Drennan, P. G. Black, and J. R. French, 2007: Turbulence structure of the hurricane boundary layer between the outer rainbands. *J. Atmos. Sci.*, **66**, 2455--2467.

Zhang, J. A. and M. T. Montgomery, 2012: Observational estimates of the horizontal eddy diffusivity and mixing length in the low-level region of intense hurricanes. *J. Atmos. Sci.*, **69**, 1306--1316.

Zhang, J. A., R. F. Rogers, D. S. Nolan, and F. D. Marks Jr., 2011: On the characteristic height scales of the hurricane boundary layer. *Mon. Wea. Rev.*, **139**, 2523--2535.

Zhuo, W., I. M. Held, and S. T. Garner, 2014: Parameter study of tropical cyclones in rotating radiative-convective equilibrium with column physics and resolution of a 25-km GCM. *J. Atmos. Sci.*, **71**, 1058--1069.